

# Ultrasonic guided wave monitoring of an operational rail track

Philip W Loveday<sup>1</sup>, Craig S Long and Dineo A Ramatio

## Abstract

An experimental monitoring system was installed on an operational heavy haul rail track. The system used two piezo-electric transducers mounted under the head of the rail to transmit and receive ultrasonic guided waves in pulse-echo mode and data were captured over a 2-week period. An artificial defect was introduced by glueing a small mass under the head of the rail at a distance of 370 m from the transducers. The size of the signal reflected by the mass varied as the glue joint deteriorated. The measurements were reordered to simulate a monotonically growing defect. The pre-processing of the captured time signals included averaging, filtering, phased array processing, dispersion compensation, signal stretching and amplitude scaling. Singular value decomposition and independent component analysis of the data were performed. Independent component analysis, with dimension reduction achieved by retaining only the larger principal components, produced the best defect detection. The defect signature was separated as an independent component, and the weight of this component increased monotonically. The results indicate that a transverse defect in the rail head could be detected and located at long range by a system comprising only two transducers. The variation of the signals due to changing environmental and operational conditions limits the size of defect that can be detected, but it is expected that even a relatively small defect, which is significantly smaller than the critical size, would be detected.

## Keywords

Structural health monitoring of rail track, guided wave ultrasound, defect detection, continuously welded rail track, singular value decomposition and independent component analysis

## Introduction

Rail operators generally perform periodic inspection of the rail track using inspection cars with conventional ultrasonic testing systems, magnetic induction systems and sometimes a combination of ultrasonic and electromagnetic testing.<sup>1</sup> These inspections aim to detect cracks of a small size to ensure that the crack will not grow sufficiently to cause a rail break before the next inspection is performed. In spite of these efforts, rail breaks do occur and the effectiveness of rail defect management strategies is measured by the ratio of detected defects to rail breaks. Typically, 10–20 defects are detected for every rail break that occurs.<sup>2</sup> Fortunately, only a small number of rail breaks result in train derailments.

Conventional ultrasonic inspections make use of longitudinal or shear waves that propagate in an unbounded elastic medium. When the medium is bounded, the wave propagation must satisfy the wave equations and also the boundary conditions and a number of different types or modes of wave can

propagate. Continuously welded rail track resembles a one-dimensional waveguide with a free boundary and low-frequency elastic waves can propagate along the rail direction. The presence of multiple modes of propagation and dispersion makes the interpretation of signals more complex. There are however some advantages such as the ability to interrogate a large volume of structure from a single transducer location and the ability to inspect inaccessible parts of a structure.

The use of ultrasonic guided waves has been investigated for the inspection of rail track by numerous authors. Some of these studies have been motivated by the potential of guided waves to detect smooth vertical-transverse defects in the rail head even if they

---

Industrial Sensors Impact Area, CSIR Manufacturing Cluster, Pretoria, South Africa

### Corresponding author:

Philip W Loveday, Industrial Sensors Impact Area, CSIR Manufacturing Cluster, PO Box 395, Pretoria 0001, South Africa.  
Email: [ploveday@csir.co.za](mailto:ploveday@csir.co.za)

occur under surface cracks or shelling.<sup>3</sup> Due to the lower frequencies used, the waves are not strongly scattered by large material grain size in aluminothermic welds and it is possible to detect defects within the weld.<sup>4</sup> An inspection system was developed by Imperial College and Guided Ultrasonics Ltd which could inspect buried rail at level crossings. A dry-coupled piezoelectric transducer array around the rail circumference was used to transmit and receive selected guided wave modes. The system, which operated in pulse-echo mode, could inspect 100 m of rail from one position and detect relatively small defects. Operation of trains had to be interrupted during the inspection of a line. This sophisticated system demonstrated the potential of guided wave ultrasound for the inspection of rail track. The technology used in this system was developed for inspection of pipelines in the oil and gas industry where long-range screening of pipelines was the first commercially successful application of guided ultrasound inspection. More recently, this has led to the deployment of monitoring systems. In inspection systems, the transducers and instrumentation are removed after the measurements while in monitoring systems the transducers and possibly the instrumentation are permanently installed on the structure.<sup>5</sup> This development was motivated by the costs and risks involved in accessing certain pipeline locations and also the potential for improved defect detection due to the ability to perform highly repeatable measurements and to look for growing defects.<sup>5</sup>

The occurrence of train derailments resulting from broken rails on a heavy haul rail line in South Africa prompted the development of a guided wave-based monitoring system. Trains on the Iron Export Line (ORELINE) can be 3780 m in length consisting of 342 wagons with 30t axle weight powered by locomotives distributed along the train. It was accepted that rail breaks on this line could not be eliminated completely by periodic inspections, and a system to immediately detect broken rails, transmit an alarm and stop trains was the best that could be achieved. The particular line had adopted communication-based train control (involving bidirectional train-to-wayside data communication to determine the exact position of the train) instead of track circuits, which can provide some broken rail detection capability. A guided wave ultrasound-based system using permanently installed transducers with electronics operating on solar power was developed. This system exploited the ability of certain guided wave modes to propagate long distances in continuously welded rail track. Alternate transmit and receive stations were spaced along the line and operated in pitch-catch mode. If a coded signal was not received at a receive station within a specified time interval, it was assumed that the rail had broken between the

transmit station and the receive station and an alarm was triggered to halt train operation in that section. The operating principle of the so-called Ultrasonic Broken Rail Detection (UBRD) system was simple but obtaining reliable operation without false alarms required significant effort.<sup>6</sup> The version 4 system was installed on the heavy haul line and a total of 931 transmit or receive stations were required along the 840 km long line and interrogated the entire line every 15 min.<sup>7</sup> The system effectively detected broken rails and prevented derailments justifying the capital investment.<sup>8</sup> This system is primarily a broken rail detector and when a transverse defect grows to a large size, the system can trigger alarms intermittently. These alarms are classified as false alarms, although some maintenance staff have learned that they indicate the presence of a defect and inspection of the approximately 1000 m long rail section with handheld ultrasound can then be performed to find the defect. It can also happen that a defect leads to a rail break under the locomotives of a passing train. In this case, part of the train can derail especially if additional locomotives are distributed along the length of the train. Broken rails that are successfully detected without causing a derailment still cost the operator as the line has to be closed while the break is located and a repair is made. Stopping these trains at certain locations can cause long delays as the trains cannot start again and have to be broken up and moved to a location where they are reassembled and can start moving again. These time delays result in large revenue losses. It would therefore be beneficial if the UBRD system could be upgraded to detect and locate defects prior to complete rail breaks. In the study by Loveday,<sup>9</sup> it was asked if it would be possible to combine some of the sophisticated techniques used in the inspection system<sup>4</sup> such as phased array processing with the monitoring approach. For a permanently installed system to be economically viable, it would have to monitor a long length of rail from an array of only a small number of transducers. The data obtained from such a system could be processed to detect growing defects.

In guided wave-based monitoring systems, it is often assumed that the structure is initially undamaged. Monitoring data are then analysed over time to detect the growth of defects such as corrosion patches in pipelines or fatigue cracks. If highly repeatable readings are obtained, it is possible to consider the first reading as the baseline and to compare subsequent readings with this baseline. In the technique of baseline subtraction, the first signal is subtracted from subsequent signals and the change in signal is assumed to represent damage. When the signals change due to changes in the environmental operating conditions (EOCs), the baseline subtraction becomes less effective and optimal

baseline selection and baseline stretching techniques have been proposed to reduce the influence of temperature variations.<sup>10</sup> The dominant cause of signal variations appears to be temperature changes. Techniques to partially compensate for the temperature influences by stretching the signals have been developed.<sup>11</sup> These techniques improve the performance of baseline subtraction. There are however other EOCs and effects that are not eliminated by signal stretching and these limit the performance. Recently, machine learning methods such as singular value decomposition (SVD) and independent component analysis (ICA) have been applied to separate defect signatures from environmentally induced signal variations.<sup>12–14</sup> These techniques outperformed baseline subtraction<sup>14</sup> and ICA in particular appears to perform well on pipes. In one study, monitoring and analysis by ICA produced the sensitivity five times better than that of a single inspection.<sup>5</sup>

It is anticipated that similar monitoring of rail track and analysis of the data will provide improved defect detection compared to a single inspection. The improvement obtained would be dependent on the influence of EOCs and the ability to devise compensation techniques for these effects. Temperature variations are expected to cause changes in guided wave group velocity and signal stretching may reduce this effect. Other EOCs may also cause signal variations and degrade the performance of the monitoring system. Guided wave measurements performed on operational rail track have been presented in the past.<sup>15</sup> In that work, a single measurement was performed as in the case of an inspection rather than in the situation of monitoring where a large amount of data is gathered over a period of time. A monitoring experiment was described in the study by Loveday et al.,<sup>16</sup> where data were gathered over a period of time. Initial analysis of only the pulse-echo signal obtained from a single transducer was presented in that article. This article extends that analysis to include phased array processing to analyse the rail to the left and right of the transducers separately. The processing and analysis of the resulting signals to detect defects are also significantly extended.

This article aims to show that a permanently installed guided wave ultrasound-based rail defect monitoring system could be developed at a reasonable cost per kilometre of rail, and that defect detection is possible in the presence of real EOCs.

Section ‘Monitoring signal acquisition’ describes the guided wave mode used and a two transducer system for performing pulse-echo measurements. Two transducers attached to the rail head can be used to monitor the rail for transverse defects in the rail head. An artificial defect was introduced with a varying reflection coefficient to investigate the ability of the system to detect a growing defect. The measurements performed

on an operational heavy haul rail track and data gathered over a 2-week period are described. Section ‘Signal pre-processing’ describes the signal processing performed on the time-domain signals including phased array processing, dispersion compensation and signal stretching to compensate for temperature-induced changes in group velocity. The analysis of these signals using machine learning techniques is presented in section ‘Defect detection’.

## Monitoring signal acquisition

This section provides details of the monitoring experiment that was performed. The mode of guided wave propagation used and the monitoring system are briefly described. Details of the rail section that was monitored and the artificial defect that was used are provided.

### Guided wave mode selection

Design of a guided wave inspection or monitoring system starts with the selection of appropriate modes of propagation. The selected modes should interact with the defects to be detected, should be easy to excite and sense and should preferably have low dispersion. In the case of long-range monitoring of rail, the modes should have low attenuation so that energy can travel long distances to detect defects at large distances from the transducers.

The modes that propagate in a one-dimensional waveguide with arbitrary but constant cross-section can be efficiently computed using the semi-analytical finite element (SAFE) method. The finite element formulation presented by Gavrić<sup>17</sup> was used. Three modes of propagation which propagate with relatively low attenuation and have energy concentrated mainly in the rail head have been identified in previous studies. These modes may be excited by a transducer attached under the head of the rail and have been used to estimate the rail material and geometric properties in a recent study.<sup>18</sup> The three modes are shown in Figure 1. In a symmetric rail profile, two of these modes ( $s_3$  and  $s_7$ ) are symmetric while the third mode ( $a_{11}$ ) is antisymmetric. The mode numbering scheme proposed in the study by Loveday et al.<sup>19</sup> is used.

Of the three modes, the symmetric mode with motion in the vertical direction ( $s_3$ ) has the least dispersion and has been found to propagate with relatively low attenuation. Numerical modelling has shown that this mode reflects strongly from transverse defects in the rail head. A transducer has previously been developed to transmit and receive this mode and two of these transducers were used in this experiment.

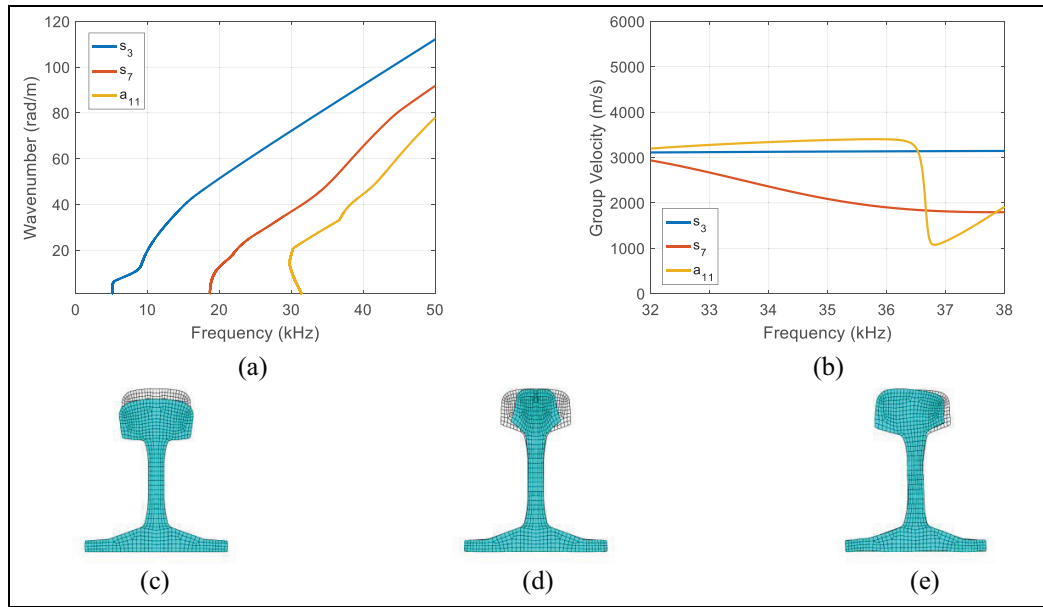


**Figure 1.** Dispersion characteristics of selected head modes computed using SAFE modelling: (a) wavenumber, (b) group velocity, (c)  $s_3$  mode shape, (d)  $s_7$  mode shape and (e)  $a_{11}$  mode shape.

### Monitoring system hardware and software

The piezoelectric transducers used had been designed to effectively excite the selected mode of propagation around 35 kHz. The sandwich transducers were designed using numerical modelling of the transducer (represented by a three-dimensional finite element model including piezoelectric elements) coupled to the rail (represented by a SAFE model).<sup>20,21</sup> This transducer design was optimized manually, although it is possible to apply more rigorous optimization techniques as was performed in the study by Ramatlo et al.<sup>22</sup> Figure 2(a) shows two of these transducers attached under the head of the rail. The spacing between the centres of the two transducers was approximately 25 mm. Preferably, the transducers should be one quarter of the wavelength apart, which would be 19.2 mm for the selected mode at 35 kHz. This was not possible because of the size of the transducers and the jig used to glue the second transducer in place. The phased array processing uses the actual spacing to apply the correct phases over the frequency range used so this is not a serious limitation. A third transducer was attached to the web of the rail but data from this transducer are not considered in this study.

The monitoring electronics was housed in a steel box within a cabinet next to the rail track, as shown in Figure 2(b) and (c). Electrical alternating current (AC) power was available in this cabinet and a battery and battery charger were installed to provide uninterrupted supply of 12 V. The transducers were connected to the electronics by cables. The electronics included a diode-

based pulse-echo circuit, a drive amplifier, a data acquisition system and a single-board computer with 3G modem. The drive amplifier used was a PiezoDrive MX200 which could generate signals between 0 and 200 V, which was one quarter of the allowed drive voltage range for the transducers which was -400 to 400 V. The data acquisition system was a NI CompactDAQ, which had a four-channel digital-to-analogue converter (NI 9263, 100 kHz, 16 bits,  $\pm 10$  V) for generating the signal, a four-channel analogue-to-digital converter for receiving signals (NI 9215, 100 kHz simultaneous, 16 bits,  $\pm 10$  V), a relay module (NI 9481) to apply the drive excitation to different transducers and a temperature module (NI 9211) to measure the temperature inside the cabinet. A single-board computer was mounted on the outside of the box and was used to control the measurements, as shown in Figure 2(c). A 3G modem was installed on the single-board computer and was used to transmit captured data to a server. The section of rail used had aluminothermic welds spaced approximately 240 m apart and the transducers and artificial defect were placed away from these welds, as illustrated in Figure 2(d).

Software was written in MATLAB and made use of the Data Acquisition Toolbox. Timers were used to schedule various activities. The 3G modem was used to send data files to a remote server and to download a configuration file, used to change measurement system parameters, from the server. Initially, the measurements were performed periodically and the data were stored.

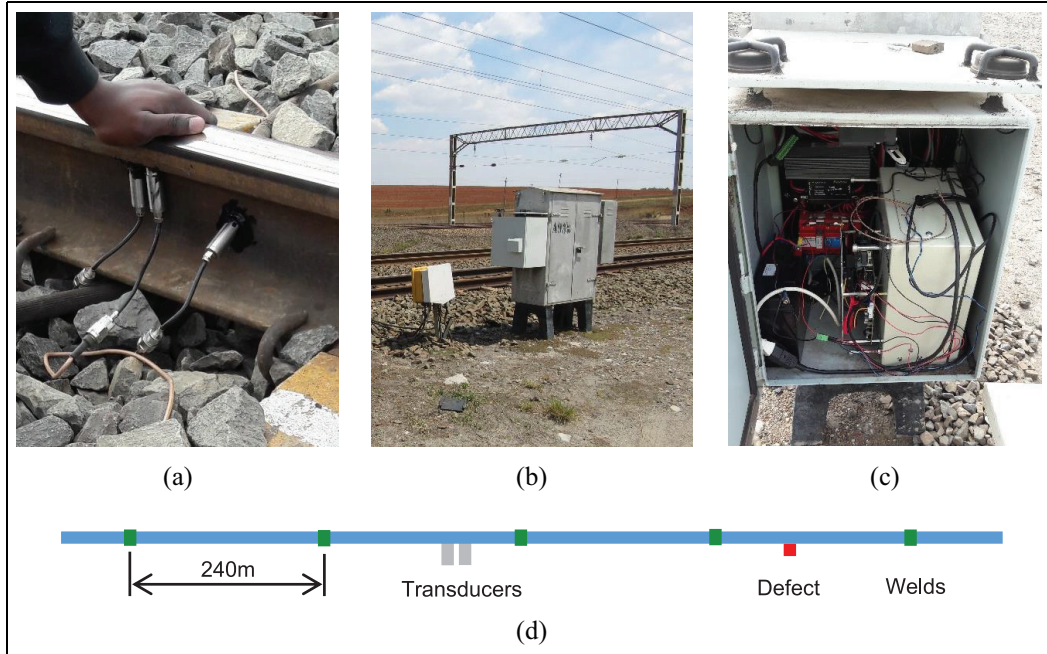


**Figure 2.** Rail monitoring equipment: (a) transducers, (b) wayside cabinet, (c) monitoring electronics and single-board computer and (d) track layout illustration.

Later, the measurements were preceded by measurement of noise to detect the presence of trains. If a train was detected, then the measurements were postponed until the train noise had disappeared.

### Artificial defect

There are numerous categories of defects that occur in rail track. One of the common defects in the rail head is the transverse defect, as illustrated in Figure 3(a). Such a defect can originate from an inclusion in the rail head and fatigue causes the crack to grow until it reaches a critical size where the rail breaks. It is expected that the reflection of ultrasonic guided waves would increase monotonically as the crack propagates. The crack growth rate and the defect size at failure are strongly dependent on multiple parameters.<sup>23,24</sup> The ability of guided wave ultrasound to detect defects should ideally be demonstrated by detecting real growing cracks in operational rail lines. This was not possible because even small cracks detected by conventional ultrasound inspections are removed from the heavy haul line that was available for our measurements. It was therefore necessary to introduce an artificial defect. In laboratory experiments, researchers often introduce defects by machining holes or slots but this is not permitted on a rail track. Instead, a small mass was glued to the rail to cause a small reflection of ultrasonic energy. The mass of 17.5 g is shown attached to the rail in Figure 3(b).

During the development of the transducers used in this experiment, a glue joint and procedure were developed and transducers have been attached to the rail for over 2 years. In the case of the defect, it was desired that the glue joint would degrade relatively quickly to provide a time-varying reflection. The mass was simply bonded to the rail using cyanoacrylate (superglue) and the joint was not protected from corrosion. It was expected that the joint would weaken in a few weeks and that the mass would fall off and that the monitoring system would detect this. The order of the data captured could then be reversed before analysis to represent a monotonically growing defect to simulate the growth of a fatigue crack.

The size of the mass used to represent the crack was selected to provide a realistic reflection. A hybrid numerical modelling technique<sup>25</sup> was used to model the reflection of the selected guided wave mode by an aluminothermic weld and by an attached mass. The attached mass was predicted to provide a displacement reflection coefficient of approximately 0.04 which would be similar to that obtained from a weld. A semi-circular transverse crack, with a radius of 5 mm, at the top of the rail head was previously predicted to reflect slightly more than an aluminothermic weld.<sup>26</sup> This modelling assumed that the mass was rigidly bonded to the rail and was expected to overestimate the reflection that would be obtained. Therefore, the selected mass reflector was expected to reflect similarly to a small transverse crack in the head of the rail.

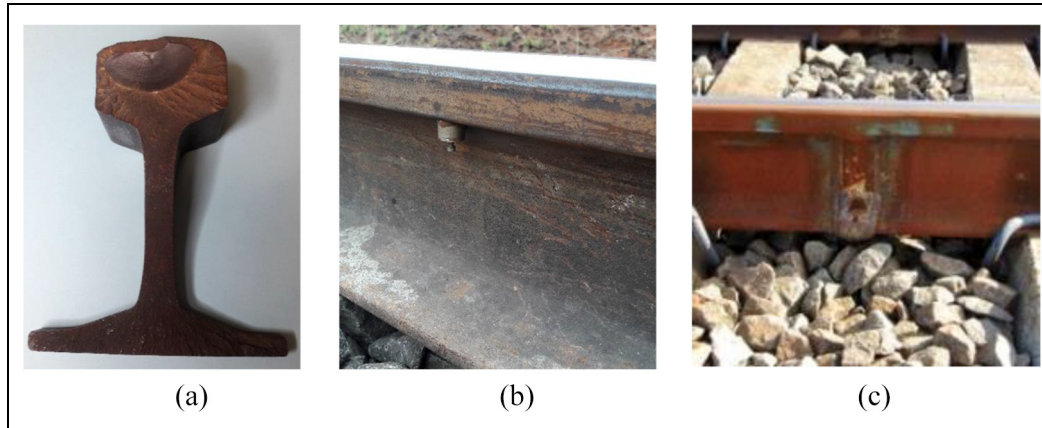


**Figure 3.** Photographs of rail defects and features: (a) a transverse defect that caused a broken rail, (b) mass glued to rail and (c) typical aluminothermic weld.

The continuously welded rail track is made up of 60 m length of rail. Four of these 60 m lengths of rail are flash butt welded together in a factory and no visible weld cap remains. These flash butt welds do not cause a detectable reflection of the guided waves and these welds are not considered in this article. The term weld used in the remainder of this article should be understood to mean aluminothermic weld. The 240 m length welds are installed in the field using aluminothermic welding which produces a weld cap which is ground off the top and sides of the rail head but remains in place around the remainder of the rail circumference. An example of such a weld is shown in Figure 3(c). The reflections from these welds can provide useful information during guided wave testing. The reflection of guided waves by these welds has been compared to the predicted reflection for a transverse defect by numerical modelling,<sup>26</sup> and it is believed that if these welds can be detected, then a crack will be detected well before it reaches the critical size to cause a broken rail.

## Signal pre-processing

The excitation signal used was a 17.5-cycle Hanning-windowed tone burst centred at 35 kHz. This signal was generated in the data acquisition system and then amplified to have peak-to-peak maximum amplitude of 200 V. The relay module was used to apply this signal to either the first or the second transducer. Each measurement set was performed by first exciting the first transducer and measuring the response of both transducers and second exciting the second transducer and measuring the response on both transducers. A sampling frequency of 100 kHz was used. The measurements were each repeated 10 times and the average of the 10 measurements was stored for each measurement

set. Therefore, four time signals were produced in each measurement set. This is the two transducer case of full matrix capture.<sup>27</sup>

Initially, the system was programmed to perform a measurement set every 30 min. It was found that the measurement performed in this manner often contained noise from passing trains and the programme was modified to first listen for train noise and to delay the measurement set until there was no train noise. The data were captured over a 2-week period and stored on the computer. Limited data were transmitted to the remote server and analysed during the 2-week period. In total, 488 measurement sets were obtained without train noise and the analysis for these measurements is presented in this article.

Before attempting to detect or monitor the defect in the data, pre-processing was performed and the steps are illustrated in Figure 4 and described in sections ‘Phased array processing’, ‘Dispersion compensation’, ‘Signal stretching and scaling’ and ‘Signal reordering to simulate monotonic defect growth’. The pre-processing of the data involved phased array processing, dispersion compensation, signal stretching and scaling and reordering of the signals. The pre-processing steps are required to determine the direction of the reflections, to reduce the influence of dispersion and to compensate for some of the environmental changes that occur.

Typical signals before and after the addition of the artificial defect are shown in Figure 5(a). The excitation signal was centred at 35 kHz and contains little energy outside of the frequency range of 32–38 kHz. During the pre-processing, the signals are converted to the frequency domain and only the content between 32 and 38 kHz was processed. This is effectively a filtering step and the example signals are shown in Figure 5(b) with this filtering. It is clear that the filtering reduced the

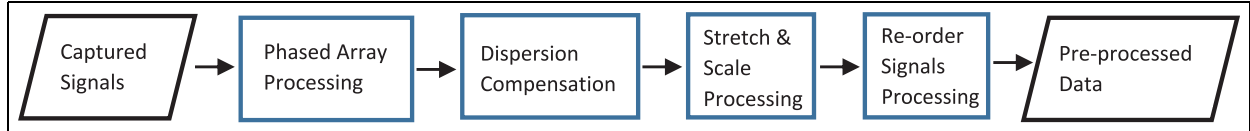


**Figure 4.** Steps involved in the pre-processing of the captured signals.

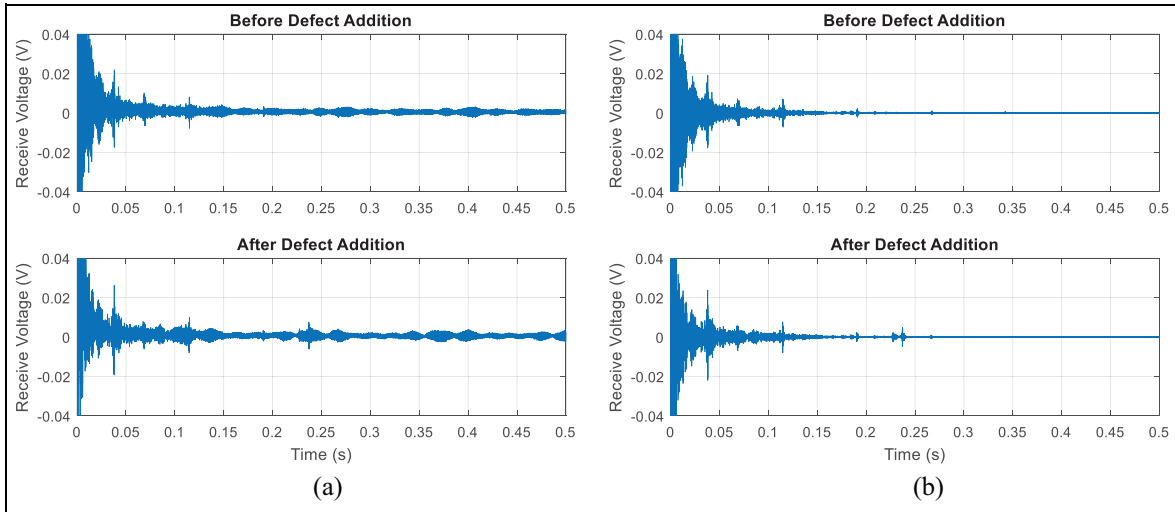


**Figure 5.** Example measured signals: (a) before and after defect addition and (b) frequency band filtered signals before and after defect addition.

noise in the signals making the reflections easier to see. Various reflections from aluminothermic welds are visible and the reflection from the artificial defect is visible between 0.23 and 0.24 s.

### Phased array processing

When an array of transducers is available, it is possible to target specific modes and directions of wave propagation. In the simple case of two transducers spaced along the axis of the waveguide, it is possible to excite both transducers with a small delay or phase difference between the two excitation signals to preferentially transmit energy in one direction along the waveguide. The phase difference would depend on the wavelength of the mode of propagation to be transmitted at that frequency and the axial distance between the two transducers. For example, if the transducers are spaced apart by a distance of one quarter of the wavelength and the two excitation signals are 90° out of phase, then the two excitations would cancel in one direction and add in the other with the result that energy is only transmitted in one direction along the waveguide. The same principle applies to receiving so by applying a phase difference to one transducer signal, it is possible to receive energy in the one mode from only one direction. It is important

to note that other modes with different wavelengths would be transmitted and received in both directions as the perfect cancellation is not possible. In order to separate more than one mode in two directions, additional transducers would be required.

Wilcox explained how phased array processing may be applied to the full matrix of captured signals obtained from a transducer array.<sup>28</sup> The captured time signals are converted to the frequency domain where the processing is performed and the processed signals may be converted back to the time domain later. When the first transducer is excited, the response captured on both transducers is stored in the first column of the matrix, and when the second transducer is excited, the responses are stored in the second column as shown in equation (1)

$$V(\omega) = \begin{bmatrix} \left\{ V_1(\omega) \right\}^{Ex1} & \left\{ V_1(\omega) \right\}^{Ex2} \\ \left\{ V_2(\omega) \right\}^{Ex1} & \left\{ V_2(\omega) \right\}^{Ex2} \end{bmatrix} \quad (1)$$

Mode shape matrices are required to analyse different combinations of transmitted and received modes of propagation. The modes selected for receive processing may be different from those selected for transmit processing. The receive mode shape matrix and the transmit mode shape matrix are shown in equation (2)

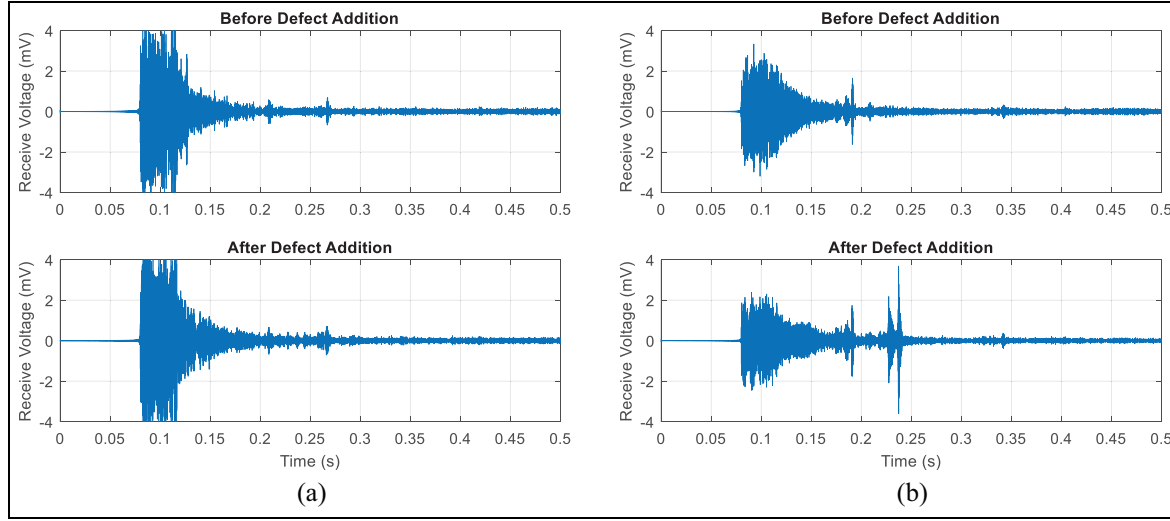


**Figure 6.** Time-domain signals after phased array processing: (a) transmitting to the left and receiving from the left and (b) transmitting to the right and receiving from the right.

$$R(\omega) = \begin{bmatrix} \psi_{1r_1} e^{-j\kappa_{r_1}(\omega)z_1} & \psi_{1r_2} e^{-j\kappa_{r_2}(\omega)z_1} \\ \psi_{2r_1} e^{-j\kappa_{r_1}(\omega)z_2} & \psi_{2r_2} e^{-j\kappa_{r_2}(\omega)z_2} \end{bmatrix} \quad (2)$$

$$T(\omega) = \begin{bmatrix} \psi_{1t_1} e^{-j\kappa_{t_1}(\omega)z_1} & \psi_{1t_2} e^{-j\kappa_{t_2}(\omega)z_1} \\ \psi_{2t_1} e^{-j\kappa_{t_1}(\omega)z_2} & \psi_{2t_2} e^{-j\kappa_{t_2}(\omega)z_2} \end{bmatrix}$$

The terms in these matrices are obtained from the SAFE analysis of the rail. The term  $\psi_{1r_1}(\omega)$  is the element in the mode shape vector for receive mode 1 at the location and direction corresponding to transducer 1 at frequency  $\omega$  and  $\kappa_{r_1}(\omega)$  is the wavenumber of receive mode 1. The axial locations of transducers 1 and 2 are  $z_1$  and  $z_2$ , respectively. If the same modes are selected for receiving and transmitting, then  $R = T$ . In this article, mode  $s_3$  shown in Figure 1 was used in the forward and backward direction as the two modes for both receiving and transmitting. The two transducers used in this work were mounted at the same circumferential location and in the same orientation, so the  $\psi$  terms could all be set to 1 and  $z_1$  was set to 0 while  $z_2$  was set to the spacing between the transducers.

The mode shape matrices and the captured matrix are used in equation (3) to compute the response of the different mode combinations. These mode combinations are shown in equation (4)

$$\alpha(\omega) = R(\omega)^{-1} V(\omega) T(\omega)^{*} \quad (3)$$

$$\alpha(\omega) = \begin{bmatrix} \alpha_{r_1 t_1}(\omega) & \alpha_{r_1 t_2}(\omega) \\ \alpha_{r_2 t_1}(\omega) & \alpha_{r_2 t_2}(\omega) \end{bmatrix} \quad (4)$$

Transmission in the forward direction and receiving in the forward direction is the first element,  $\alpha_{r_1 t_1}(\omega)$ , which ideally would be zero. Transmission in the

forward direction and receiving in the backward direction,  $\alpha_{r_2 t_1}(\omega)$ , should show reflections from features in the forward direction. Reflections from features in the backward direction would be seen in  $\alpha_{r_1 t_2}(\omega)$ . The results shown in Figure 6 are for the two mode combinations that should show reflections. Some calibration factors were introduced to take into account the different sensitivities of the two transducers.

As shown in Figure 6, the results for phased array processing are shown for signals before and after the defect was added. Reflections from welds in the two directions are visible in the left and right figures. Note that the addition of the defect introduces a large reflection in the one direction and not in the other. This indicates that the phased array processing is effective. The first parts of the signals have been zeroed as these regions contain significant energy from other modes and reflections from rail supports and the phased array processing, which is based on only one mode propagating in two directions, is ineffective in this situation.

### Dispersion compensation

Although a mode with relatively little dispersion was selected, the influence of dispersion is noticeable due to the long ranges of propagation. Dispersion compensation was performed using the algorithm developed by Wilcox<sup>29</sup> and dispersion data from the SAFE model. This process also converts the signals from the time domain to the distance domain so that the actual distances of various reflectors can be viewed directly. Example signals are shown in Figure 7 where the signals interrogating the rail to the left of the transducer are plotted in Figure 7(a) and those interrogating the rail to

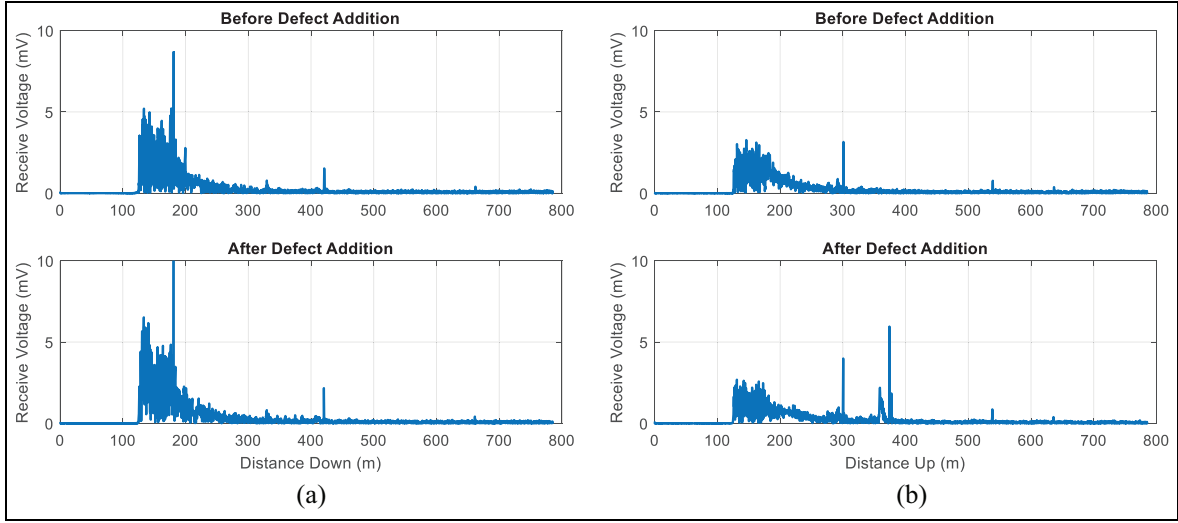


**Figure 7.** Dispersion compensated signals before and after defect addition: (a) in the down direction and (b) in the up direction.

the right of the transducers are shown in Figure 7(b). In these figures, the envelope of the signal is plotted and the distance is denoted either as Distance Down, for the direction of train travel down to the coast, or as Distance Up, for the opposite direction. The early part of the time signals was zeroed as welds or defects in this region would not be detected. The plot shows reflections from aluminothermic welds at 180, 420 and 660 m in the down direction and at 300, 540 and 640 m in the up direction. The location of these welds was confirmed by visual inspection of the rail track. The large defect reflection is shown in Figure 7(b). The peak of the reflection is at 374 m but because of the multi-modal and dispersive nature, the reflection extends from 358 to 380 m. This is more clearly visible in Figure 9(d).

### Signal stretching and scaling

In a defect-free rail, the signals gathered would vary over time due to changing EOCs. Compensation techniques to reduce the effects of EOCs in pipe and plate systems have been developed. For this rail track, these compensation techniques may or may not be appropriate and additional compensations may be required. The purpose of compensation is to reduce the variations of the defect-free signals. Naturally, the compensation techniques must not remove the influence of the defect to be detected.

The group velocities of guided wave modes vary with varying temperatures. This causes the reflections to appear to shift in time or distance when measurements are performed at different temperatures. The shift of reflections from benign features makes a simple baseline subtraction much less effective<sup>30</sup> and would also degrade the performance of the defect detection

techniques used in section ‘Defect detection’. The influence of this EOC can be reduced by compensating for the change in group velocity by stretching the signals. Techniques have been developed and applied to pipe and plate monitoring.<sup>11</sup> The signals can be stretched either in the time domain or in the distance domain. Stretching in the time domain distorts the wave packet and introduces a small frequency change<sup>10</sup> and stretching in the distance domain seemed more natural; although for a mode without dispersion, the result would be the same. Dispersion compensation was performed first to reduce the distortion of the wave packets that occurs especially over the long distances being considered. The dispersion compensation also converts the signals from the time to the distance domain; therefore, the stretching was performed in the distance domain.

Two signals from measurements performed at different temperatures are shown in Figure 8(a). It is noted that the influence of temperature change is large on these signals due to the long-range propagation and also the fact that the signals contain more than one mode. The change is not a simple phase shift and the wave packet envelope also becomes distorted. The scale-invariant correlation technique developed by Harley and Moura<sup>11</sup> was applied to these signals but did not produce satisfactory results. Instead, a piecewise linear stretch of the wave envelope signals was used to align the wave envelope peaks at each weld reflection location. The wave envelopes are used and the phase information is discarded. In this approach, the presence of the weld reflections is actually useful as they provide the stretch factors. The stretching process is illustrated in Figure 8 for weld reflections in the up and down directions.

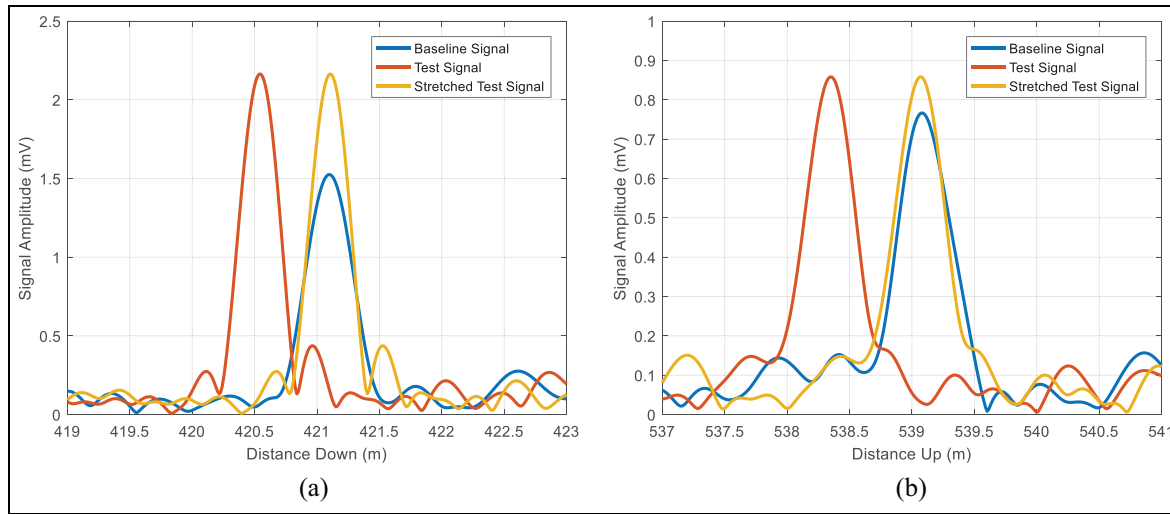


**Figure 8.** Stretching of signal envelopes to align with the peaks of the baseline signal, examples: (a) in the down direction and (b) in the up direction.

The amplitude of the signals also varies during the monitoring period as can be seen in Figure 8. This could be due to the sensitivity of the transducers varying with temperature or the attenuation of the rail changing with temperature or as the rail gradually sinks into the ballast. Signal scaling can be performed to reduce this by scaling the weld reflection peaks. One weld in each direction (420 m down and 300 m up) was used to scale the signals so that all the signals have the same peak amplitude for this reflection.

The attenuation of the guided waves with distance makes the further weld reflections appear smaller, as shown in Figure 7. An energy-based normalization was applied to each signal envelope using the technique described by Moustakidis et al.<sup>31</sup> A moving average was used to define an energy attenuation measure that was used in the normalization.

The phase of the signals was previously discarded and only the envelope remains. The ICA did not work well on these signals which have large direct current (DC) components. For this reason, the wave envelope signals were multiplied by a single-frequency sine wave. This produced signals suitable for ICA. Figure 9 shows example signals after stretching and scaling. Note that the two signals shown in Figure 9(c) have the same phase because both envelopes were multiplied by the same single frequency sine wave to produce these signals. The analysis that is performed in section ‘Defect detection’ is therefore really an analysis of the envelopes of the signals.

Figure 9(d) shows the nature of the reflection caused by the artificial defect. The main reflection centred at approximately 375 m is due to mode  $s_3$  arriving at the defect and reflecting as mode  $s_3$ . The earlier arrival,

between 358 and 370 m, is thought to be due to mode  $s_3$  arriving at the defect and reflecting as mode  $a_{11}$ , which has higher group velocity and has greater dispersion (see Figure 1) causing the wave packet to be elongated. The later reflection at 378 m is suspected to be due to mode  $s_3$  arriving at the defect and being reflected as another mode, which is not included in Figure 1.

#### *Signal reordering to simulate monotonic defect growth*

The size of the reflection caused by the artificial reflector varied greatly over time. In Figure 10(a), the peak amplitude of the signal in the distance range of 370–385 m was found and plotted against the test number. It had been expected that the reflection would decrease monotonically as the glue joint deteriorated but this was not the case, as shown in Figure 10(a). The defects to be detected in a rail track are expected to increase monotonically and the tests were therefore reordered in order of increasing defect reflection. The peak reflection for the new order is shown in Figure 10(b). These signals are used for defect detection in the next section.

The reflection obtained from the artificial defect may be compared to that obtained from a weld. The dispersion compensated signals for the largest reflector signal, the 300th sample and the smallest reflector signal are shown in Figure 10(c). The signals in Figure 10(c) and (d) do not contain any stretching nor energy scaling, and therefore, the peak amplitudes are different to those shown in Figure 10(a) and (b), which included energy scaling. The size of these reflections is compared to that which would be expected if a weld was located

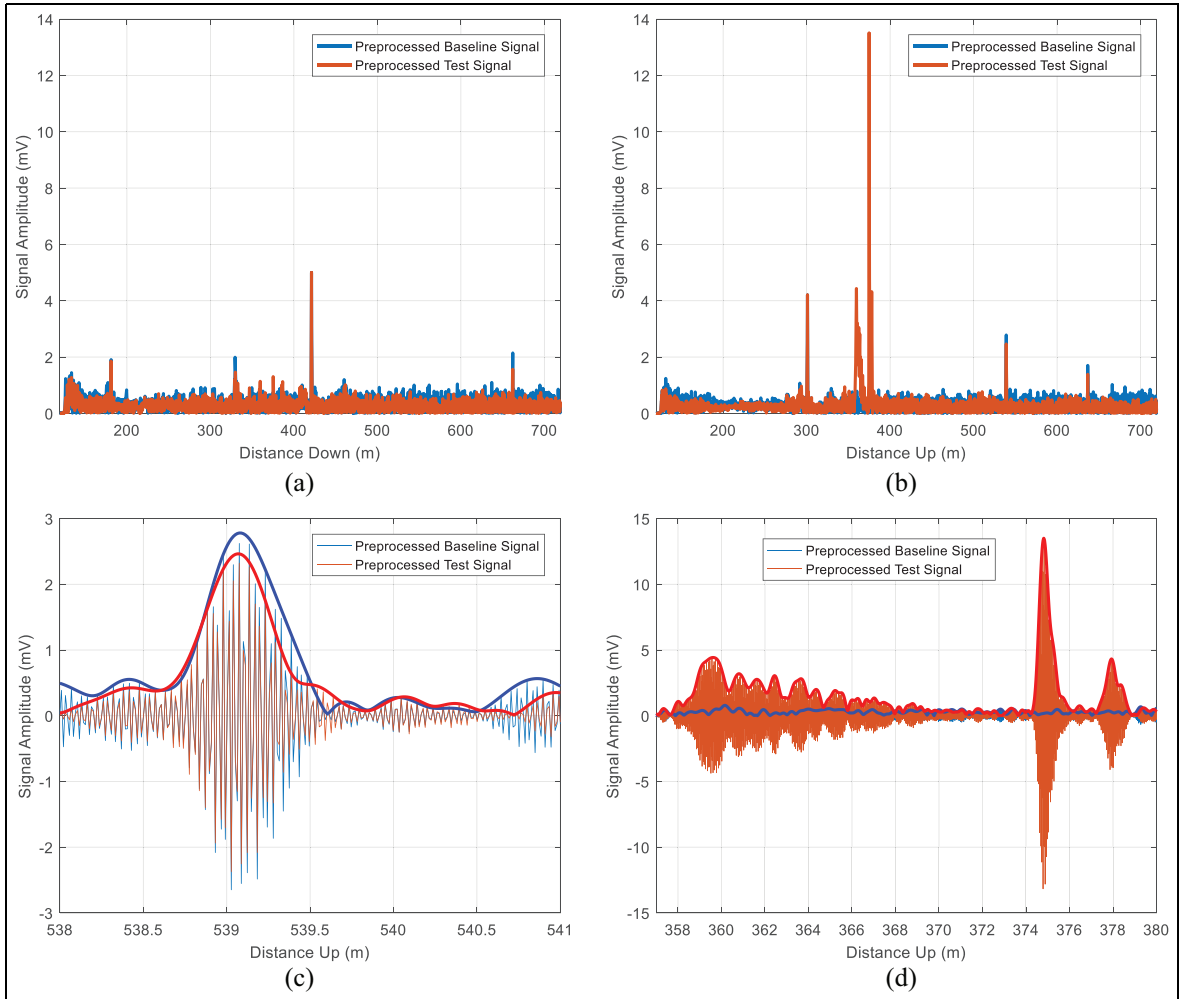


**Figure 9.** Pre-processed signals available for defect detection: (a) envelopes of signals in the down direction and (b) up direction, (c) envelopes and sine signal for a reflection in the up direction and (d) baseline and test signal reflection at the artificial reflector.

at the same distance in Figure 10(d). An exponential function is fitted between the two weld reflections at 300 and 540 m and this is used to estimate the size of a weld reflection for a weld located at 375 m, which is the location of the artificial defect. It is seen that in the case of the largest defect reflection, this reflection is approximately three times larger than a weld reflection while for the 300th sample, the defect reflection is approximately one-third of a weld reflection. Numerical modelling was previously used to compare the reflections expected from transverse cracks in the head of the rail to those expected from welds.<sup>26</sup> A crack reflecting three times more than a weld would be expected to have an area of approximately 150 mm<sup>2</sup>. While this may appear large, there are many photographs, in the literature, of broken rail which have fatigue cracks with the larger area before the break occurred. A crack would be expected to be smaller than 20 mm<sup>2</sup> in area to provide

a reflection one-third of the size of a weld reflection. It is believed that it would be more than acceptable if a continuous monitoring system could detect a crack of this size.

## Defect detection

Various techniques may be applied to detect the presence of a defect or the growth of a defect in the pre-processed data. The techniques applied in this article are described in section ‘Defect detection techniques’. In section ‘Defect detection including large defects’, these techniques are applied to all the monitoring data (all 488 samples), which include samples with large defect reflections. Finally, in section ‘Detection of growing small defect’, the techniques are applied to the first 300 samples so that the data set only includes samples where the defect reflection is relatively small.

## Defect detection techniques

Defect detection would be simple if only the defect caused a change in the measured signals. In this case, subtraction of the current measured signal from a baseline signal (assumed to be free of defects) would reveal the defect signature. Unfortunately, EOCs cause significant changes in the signals measured even on an undamaged structure and simple subtraction is not effective. Optimal baseline and baseline stretch techniques have been shown to reduce the influence of EOCs. More recently, data-driven approaches have been investigated. Two machine learning techniques, SVD and ICA have yielded promising results for monitoring of plates<sup>12</sup> and pipes,<sup>13</sup> respectively. The SVD and ICA techniques outperformed the baseline subtraction technique when applied to detect simulated defect signatures superimposed on measured data from a pipe subjected to EOCs.<sup>14</sup> These techniques are described briefly in this section before they are applied to the data.

The set of 488 pre-processed measurements were stored as rows of the data matrix  $X$ , which has dimension  $m \times n$ , where  $m$  is the number of measurements performed and  $n$  is the number of voltage values in a single measurement. This data matrix is represented as the linear transformation shown in equation (5)

$$X = A \cdot C \quad (5)$$

where the matrix  $A$  represents the trends in the data over the monitoring period and matrix  $C$  represents the components of the data over the measurement distance.

Liu et al. (2015) demonstrated that SVD can perform this function. Equation (6) shows that SVD of the real data matrix  $X$  produces the left singular vector matrix  $U$ , the diagonal singular value matrix  $S$  and the right singular vector matrix  $V$

$$X = U \cdot S \cdot V^T \quad (6)$$

Matrices  $U$  and  $V$  are orthogonal matrices and the columns of  $U$  represent different trends in the data over slow time while the columns of  $V$  form an orthonormal basis for the signals in fast time (or distance in this article). Furthermore, each pair of left/right singular vectors contain one component of the variation of the data in slow/fast time, respectively. The singular values (which are the diagonal of matrix  $S$ ) are ordered in descending order. The magnitude of each value indicates the amount of information in the data matrix which is contained in the associated left and right singular vectors. Small singular values contain negligible information and may be discarded either to reduce the dimension of the data or to de-noise the data.

ICA provides another representation of the data matrix in the form of equation (5). ICA attempts to separate the data matrix into a defined number of independent components (columns of matrix  $C$ ) which have the minimum statistical correlation between the components. Here, matrix  $A$  contains the independent component weights. ICA is useful for separating different sources, and here, it is applied to separate the contribution of a defect signature from the background signature of the system which includes the baseline signal and variations to this signal caused by EOCs. The FastICA algorithm<sup>32</sup> was used to perform the computations in MATLAB. The number of components to compute is selected by the user and there is no ranking of components in terms of importance. The algorithm is iterative and can start from a random initial set of vectors of weights. In this case, the computed components and the order of these components can change each time the computation is performed depending on the starting vector. In addition, the scaling and signs of the weight vector and associated independent component may change as only the product is important. It is possible to specify the starting vector so that repeatable results are obtained.

The FastICA algorithm first normalizes the data set in steps known as demeaning and whitening. The whitening step involves computation of the principal values and components (eigenvalues and eigenvectors of the covariance matrix  $X \cdot X^T$ ). An option is provided to retain only a selected set of the principal components.

In section ‘Defect detection including large defects’, we plot independent component weights and components. The components are scaled so that the magnitude of the largest term in the vector is equal to one or the peak of the ultrasonic signal is set to unity. The corresponding weight is also scaled by the inverse of this scaling so that the product of the weight and the component remain unchanged. We perform a similar scaling on the singular vectors computed by SVD. The right singular vector is scaled so that the peak of the ultrasonic signal is set to unity. The left singular vector is scaled by the inverse of this factor and multiplied by the singular value. In this way, the results from SVD and from ICA may be directly compared.

## Defect detection including large defects

The complete set of 488 measurements were analysed in the reordered sequence. This data set represents a monotonically growing defect, which reaches a large size, as illustrated in Figure 10.

SVD. The first eight left and right singular vectors are shown in Figure 11 for the signals received from each

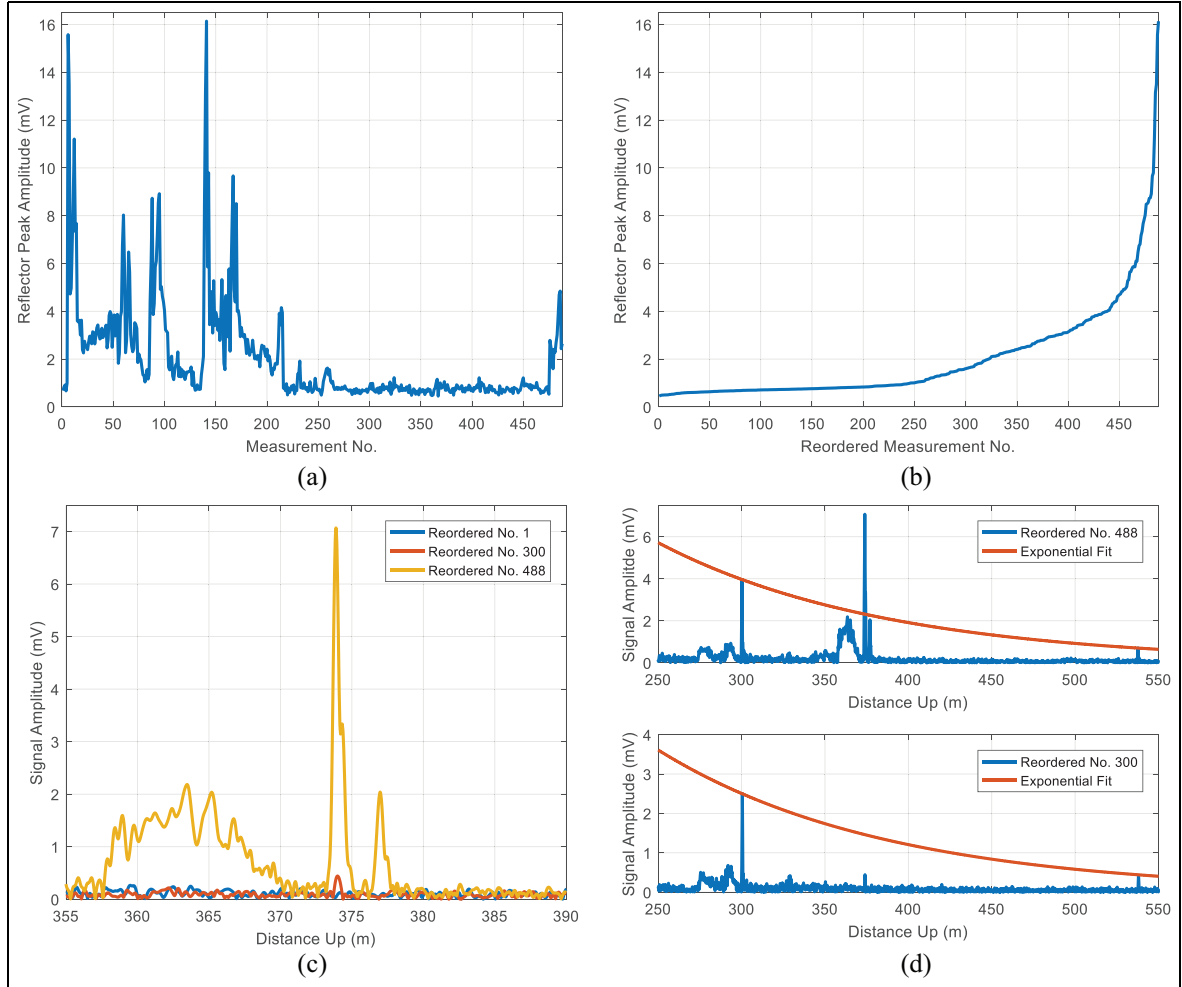


**Figure 10.** Reordering of the measurements to simulate monotonic defect growth: (a) artificial reflector peak amplitude during measurement period, (b) reordered measurements to provide monotonic growth of reflection peak, (c) artificial reflections in selected measurements and (d) artificial reflection peak compared to exponential fit of weld reflections.

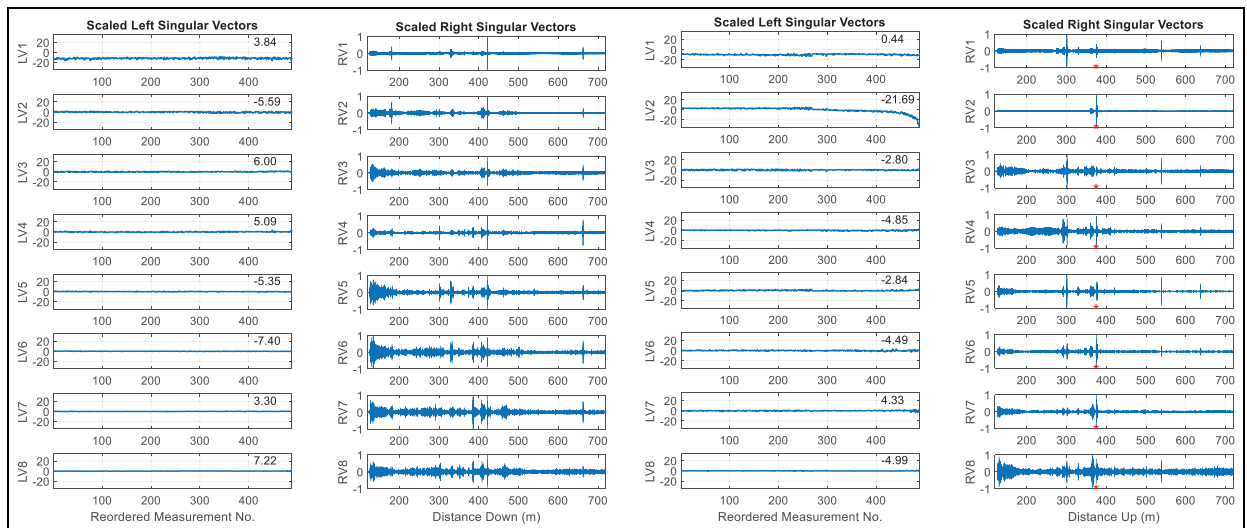


**Figure 11.** First eight left and right singular vectors of the complete data set in the down (left) and up (right) directions.  $Z_{mk}$  values are inserted on the scaled left singular vectors.

**Table I.** Mann–Kendall test scores for analyses of complete data set.

Weight no.	SVD down	SVD up	ICA down	ICA up	DR–ICA down	DR–ICA up
1	3.84	0.44	3.65	0.81	2.03	7.93
2	-5.59	-21.69	-5.74	-24.37	-5.56	-24.48
3	6.00	-2.80	1.81	1.03	2.45	-1.98
4	5.09	-4.85	1.17	14.01	10.70	15.68
5	-5.35	-2.84	-6.98	7.97	-0.07	-18.55
6	-7.40	-4.49	3.48	-18.78	0.56	5.89
7	3.30	4.33	10.89	-6.34	1.57	-11.02
8	7.22	-4.99	1.65	9.00	0.11	-4.48

SVD: singular value decomposition; ICA: independent component analysis; DR: dimension reduction.

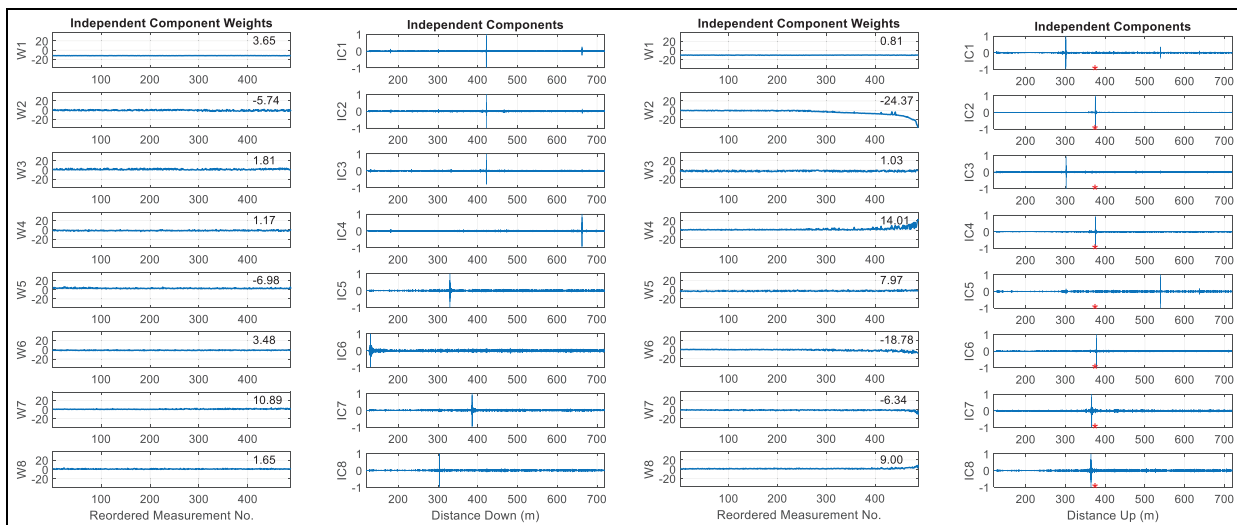


**Figure 12.** Eight weights and independent components of the complete data set in the down (left) and up (right) directions.  $Z_{mk}$  values are inserted on the independent component weights.

side of the transducers. The plots of the right singular vectors in the up direction include a small red marker at a distance of approximately 374 m, which is the location of the artificial defect. The right singular vectors resemble the ultrasonic signals (in distance) and the first right singular vector clearly shows the weld reflections. In the up direction, the first right singular vector also shows a relatively small defect reflection. The first left singular vector in either direction is largest and relatively constant. The second left singular vector of the measurements in the up direction shows a significant trend over the reordered measurements (slow time). The corresponding right singular vector resembles the ultrasonic signal that would be expected if only the artificial defect was present. There are variations in the other left singular vectors but these are smaller and may be due to temperature variations and other environmental changes.

In the study by Liu et al.,<sup>14</sup> the Mann–Kendall test was used to determine whether or not the data contain

a monotonic trend. A value  $Z_{mk}$  is computed, for each left singular vector, and if the magnitude is greater than 1.96, there is a 95% probability that there is a monotonic trend. The sign of  $Z_{mk}$  indicates whether the trend is upwards (positive sign) or downwards (negative sign). The values of  $Z_{mk}$  for the left singular vectors are displayed on the graphs and are also listed in the first two columns of Table 1. This table will be discussed later.

**ICA.** ICA was performed using the FastICA code for MATLAB.<sup>32</sup> Eight independent components were computed for the data in each direction, as shown in Figure 12. It was found that if the computation was repeated, then different components could be produced and sometimes, even components which contain significant information were not produced. This occurs because the iterative algorithm was started from a different random initial set of vectors of weights. The FastICA code allows the initial weight vectors to be

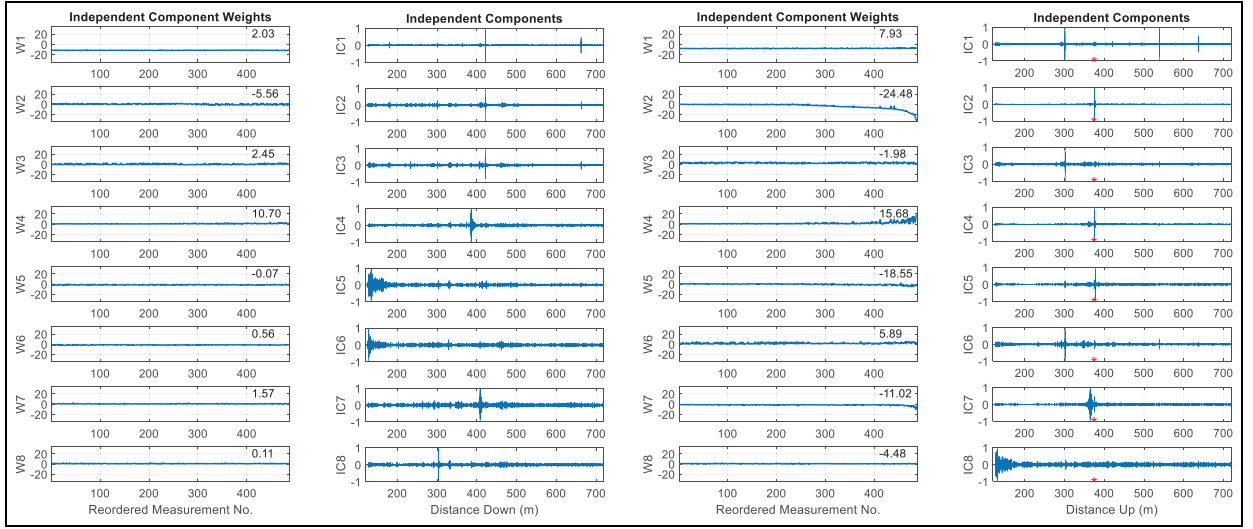


**Figure 13.** Independent component analysis of the first 60 principal components of the complete data set in the down (left) and up (right) directions.  $Z_{mk}$  values are inserted on the independent component weights.

specified for the iterative computation of the independent components. The first eight scaled left singular vectors (shown in Figure 11) were selected as the initial weight vectors. This selection means that the algorithm computes the same solution every time so that the results may be reproduced. The first independent component and weight computed will also most likely be close to the first right and left singular vector. This is indeed the case for the independent component weights, as shown in Figure 12 where the first weights in either direction are relatively constant. The first independent components in either direction show the largest weld reflection with unit amplitude, although the other weld reflections appear to have become smaller than they were in the right singular vectors. In the up direction, components 2, 4 and 6 resemble the expected defect signature at the correct distance. The weight of these components varies monotonically indicating the growing defect. In the up direction, weights 7 and 8 also show the defect growth. The components associated with these weights show the reflection at approximately 364 and 366 m and it is thought that this is caused by mode conversion at the reflector where mode  $s_7$  is incident and reflects as mode  $a_{11}$ .

The fifth component in the down direction has a significant weight. This component indicates a reflector at a distance of approximately 330 m in the down direction. There is no known feature at this location and the source of this reflection is unknown.

In general, the independent components appear to show less noise than the right singular vectors. It appears that the ICA produces a number of components each representing the reflection from one weld. It was suspected that the ICA is overfitting the

measured data. Such overfitting may be reduced by dimension reduction<sup>32</sup> and this is investigated in the next section.

**ICA with dimension reduction.** Principal component analysis (PCA) may be used for dimension reduction or noise reduction. The principal values (eigenvalues) are ordered in descending magnitude and the smaller values and associated components may be discarded. The ICA algorithm uses PCA in the whitening step and here the principal components to be retained may be selected when using the FastICA code. The first 60 principal components were retained and the FastICA algorithm produced the weights and independent components, as illustrated in Figure 13. Again, the first eight scaled left singular vectors were selected as the initial weight vectors. It was observed that the results showed little variation if the number of principal components retained was between 40 and 80. This range is likely to depend on the data being analysed and should be investigated for each data set.

The first independent component weights in both directions, as shown in Figure 13, are the largest and are fairly constant. The associated independent components again show the largest weld reflection with unit magnitude but now the reflections from other welds are larger.

The defect signature appears to be separated into components 2, 4 and 5 and the corresponding weights grow in magnitude as the defect grows. The second weight especially appears to provide a good measure of the defect growth and the component locates the defect well. The seventh weight also shows the defect growth.

It is thought that this component may be due to a faster mode of propagation reflecting from the defect and therefore, the component shows the defect location closer than the known defect location. The defect signature contains more than one guided wave mode which may be influenced differently by EOCs and this may be the reason for it being separated into multiple components.

**Trends of the weights.** When a monotonically growing defect is detected, it is expected that the weight will grow monotonically. The Mann–Kendall (M-K) test was used in the study by Liu et al.<sup>14</sup> to decide if a particular weight has a monotonic trend. The M-K test involves computing the difference between the number of increases and decreases between pairs of data points. This value is then normalized to remove the influence of the number of points in the data to produce the normalized test statistic  $Z_{mk}$ . The probability associated with falsely rejecting the null hypothesis (that there is no trend) is then evaluated using a normal distribution. If the probability of falsely rejecting the null hypothesis is set at 0.05, then values of  $|Z_{mk}| > 1.96$  would result in the alternative hypothesis being accepted (that there is a monotonic trend). Values of  $|Z_{mk}|$  which are even larger mean that the probability of falsely rejecting the null hypothesis is significantly smaller. The M-K test was performed on all the weights shown in Figures 11 to 13 to evaluate the probability of monotonic trends being present. The M-K test scores are listed in Table 1. The values in the table are large compared to those in the study by Liu et al.<sup>14</sup> (where only one weight had a value larger than 1.96) indicating that the data contain relatively large trends. This may indicate that there is a trend such as the rail sinking further into the ballast over time, even though the measurement sequence has been reordered. The size of the reflection tended to decrease during the course of the experiment, and therefore, the reordered data could still have such a trend. If the data were reordered randomly before the analyses were performed, then the  $Z_{mk}$  values were significantly smaller (generally less than 1.0).

The  $Z_{mk}$  values for the SVD left singular vectors are generally large but the second value in the up direction is significantly larger than the others. The associated right singular vector clearly corresponds to the defect signature.

When ICA was applied, the trends are again generally large but again the three weights in the up direction with the large trends (2, 4 and 6) correspond to the components resembling the defect signature. In the case of the dimensionally reduced ICA, the three weights in the up direction (2, 4 and 5) showing the largest trends

are again the components resembling the defect signature.

In the down direction, the trend for ICA weight 7 and dimensionally reduced ICA weight 4 were largest. The independent components associated with these weights are similar and show a peak at a distance of 385.5 m. It is speculated that these peaks could be due to reflection of a slower mode from the reflector. If the wavelength of this mode is different from that of mode  $s_7$ , the phased array processing may produce the incorrect direction.

### Detection of growing small defect

If the defect signature grows to a large size, it would be easy to detect and sophisticated processing would not be necessary. However, if it is required to detect the defect while it provides only a small ultrasonic signature, this is more difficult. In this section, only the first 300 ordered samples are analysed to investigate whether the techniques can detect this relatively small defect.

**SVD.** Figure 14 shows the first eight left and right singular vectors in both directions for the first 300 reordered measurements. In both directions, the first left singular vectors are large and relatively constant and the first right singular vectors resemble the ultrasonic signals without the defect. The other right singular vectors appear to be variations of this signal and the presence of the artificial defect cannot be easily observed, although it is visible in components 6 and 7 in the up direction. The M-K test results in Table 2 show the highest values for these components in the up direction. There is a higher value in the down direction for left singular value 8 so merely selecting the highest value would not provide a correct detection result in this case. In addition, analysis of the components would not be able to locate the defect.

**ICA with dimension reduction.** The first 60 principal components were retained and the first eight independent components were computed using the first eight principal component weights as the initial vector. The computed weights and independent components are shown in Figure 15.

The first independent components in both directions resemble the ultrasonic signals as would be expected and the associated weights are relatively constant. The first independent component in the up direction appears to show a small reflection from the artificial defect. The sixth independent component in the up direction appears to contain the defect signature and the magnitude of the associated weight appears to increase monotonically in a manner similar to the defect growth. This

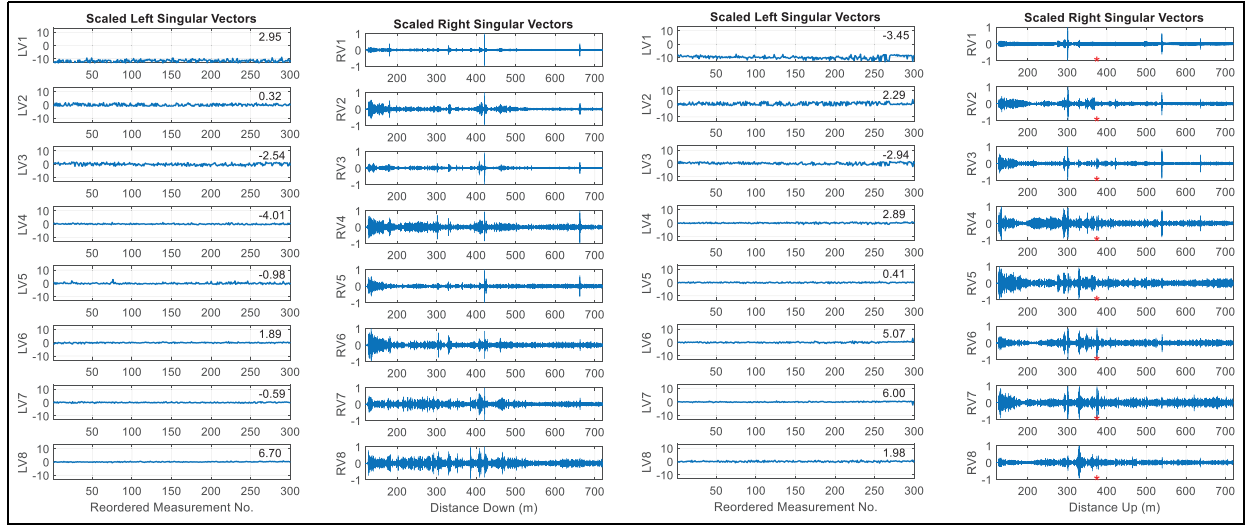


**Figure 14.** First eight weights and principal components of the first 300 ordered samples in the down (left) and up (right) directions.  $Z_{mk}$  values are inserted on the scaled left singular vectors.

**Table 2.** Mann–Kendall test scores for analyses of the first 300 ordered samples.

Weight no.	SVD down	SVD up	DR–ICA down	DR–ICA up
1	2.95	-3.45	-0.89	0.57
2	0.32	2.29	-0.24	4.35
3	-2.54	-2.94	-3.25	-0.19
4	-4.01	2.89	-1.36	2.39
5	-0.98	0.41	-0.68	1.28
6	1.89	5.07	1.30	9.63
7	-0.59	6.00	1.13	0.98
8	6.70	1.98	2.79	1.15

SVD: singular value decomposition; DR: dimension reduction; ICA: independent component analysis;

weight also has the largest trend indicated by the M-K test results in Table 2. The second weight in the up direction has the second largest trend but this value is not much larger than the rest of the values. It appears that ICA with dimension reduction performs better than SVD when attempting to detect the growth of a small defect in the presence of EOCs.

## Conclusion and recommendations

An array of only two transducers was used to monitor the head of the rail. Phased array processing was based on the most prominent mode of propagation and could not eliminate the contributions of other modes. Additional transducers would be required to achieve this. The processing correctly determined the distance and direction of reflectors.

Signal pre-processing was performed to reduce the influence of temperature variations. Other EOCs were

not compensated and relatively large variations in the signals were observed. These variations should be researched in future and compensation techniques should be developed.

An artificial defect was added and the measurements were reordered to represent a monotonically increasing defect reflection. SVD and ICA were applied to the data. The best performance was obtained when dimension reduction was performed by selecting the 60 largest principal components and performing ICA on these. The defect signature was separated from the rest of the signal and the weight showed a monotonic increase as would be expected. ICA seems to split a larger defect signature into different components and this may be because the signature contains multiple modes of propagation. This should be researched further.

Based on the results obtained, detection of relatively small defects in the rail head at long range appears to be possible with only two transducers. It is anticipated

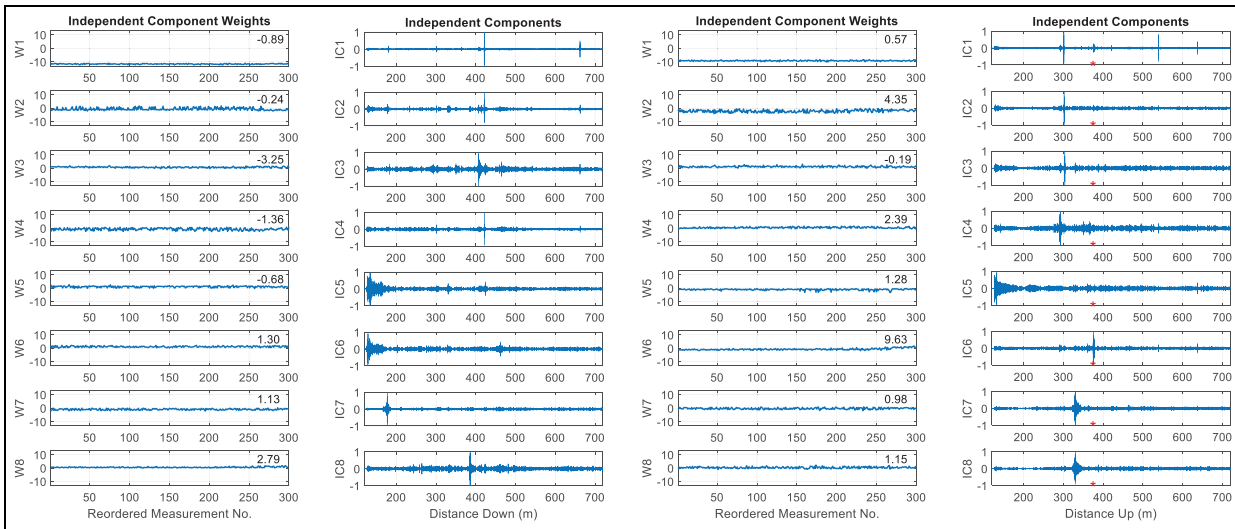


**Figure 15.** Independent component analysis of the first 60 principal components of the first 300 ordered samples in the down (left) and up (right) directions.  $Z_{mk}$  values are inserted on the independent component weights.

that significant effort would be required to develop a monitoring system that operates completely autonomously and does not produce false alarms. It is recommended that decisions to stop trains or to request a maintenance team to inspect a section of track should be made by an expert at first while data are gathered and an algorithm is developed to make such decisions. Such an algorithm could start by monitoring the size of the M-K test scores to determine whether one independent component weight has a significantly larger trend than the others. If a large trend is detected, then the associated independent component could be analysed to check that it resembles a single reflection from a defect. Finally, the magnitude of the weight and the rate of increase could be used to decide an appropriate level of alarm. Decision thresholds for these steps would be determined only once extensive data have been captured and analysed.

## Acknowledgements

The authors thank Transnet Freight Rail for providing access to the railway track and providing the cabinet for the monitoring experiment.

## Authors' note

The FastICA Version 2.5 for MATLAB was downloaded from <http://www.cis.hut.fi/projects/ica/fastica/> and used in this work.

## Funding

The author(s) disclosed receipt of the following financial support for the research, authorship and/or publication of this

article: The funding for this project was provided by the CSIR, South Africa.

## ORCID iD

Philip W Loveday <https://orcid.org/0000-0002-0515-3204>

## References

- Papaelias MP, Roberts C and Davis CL. A review on non-destructive evaluation of rails: state-of-the-art and future development. *Proc IMechE, Part F: J Rail and Rapid Transit* 2008; 222: 367–384.
- Cannon DF. Rail defects: an overview. *Fatigue Fract Eng Mater Struct* 2003; 26: 865–886.
- Hay TR, Hay DR, Plotkin D, et al. Rail defect detection under shelling. In: *Proceedings of the 7th world congress on railway research*, Montreal, QC, Canada, 4–8 June 2006, pp. 1–8. World Congress on Railway Research (WCRR).
- Wilcox P, Pavlakovic B, Evans M, et al. Long range inspection of rail using guided waves. In: *Proceedings of the review of progress in quantitative nondestructive evaluation*, vol. 22, Green Bay, WI, 27 July–1 August 2003, pp. 236–243. American Institute of Physics (AIP).
- Cawley P. Structural health monitoring: closing the gap between research and industrial deployment. *Struct Heal Monit* 2018; 17: 1225–1244.
- Burger FA. A practical continuous operating rail break detection system using guided waves. In: *Proceedings of the 18th world conference on nondestructive testing*, Durban, South Africa, 16–20 April 2012.
- Burger FA, Loveday PW and Long CS. Large scale implementation of guided wave based broken rail monitoring. In: *Proceedings of the review of progress in quantitative nondestructive evaluation*, vol. 34, Minneapolis, MN, 25–31 July 2015.

8. Duvel J and Mistry K. Improving rail integrity on the Sishen-Saldanha line. In: *Proceedings of the 11th international heavy haul association conference*, 2–6 September 2017, Cape Town, South Africa, pp. 32–39. International Heavy Haul Association (IHHA).
9. Loveday PW. Guided wave inspection and monitoring of railway track. *J Nondestruct Eval* 2012; 31: 303–309.
10. Croxford AJ, Moll J, Wilcox PD, et al. Efficient temperature compensation strategies for guided wave structural health monitoring. *Ultrasonics* 2010; 50: 517–528.
11. Harley JB and Moura JMF. Scale transform signal processing for optimal ultrasonic temperature compensation. *IEEE T Ultrason Ferr* 2012; 59: 207–224.
12. Liu C, Harley JB, Bergés M, et al. Robust ultrasonic damage detection under complex environmental conditions using singular value decomposition. *Ultrasonics* 2015; 58: 75–86.
13. Dobson J and Cawley P. Independent component analysis for improved defect detection in guided wave monitoring. *Proc IEEE* 2016; 104: 1620–1631.
14. Liu C, Dobson J and Cawley P. Efficient generation of receiver operating characteristics for the evaluation of damage detection in practical structural health monitoring applications. *Proc R Soc Lond A Math* 2017; 473: 1–26.
15. Loveday PW and Long CS. Long range guided wave defect monitoring in rail track. *AIP Conf Proc* 2014; 1581: 179–185.
16. Loveday PW, Taylor RMC, Long CS, et al. Monitoring the reflection from an artificial defect in rail track using guided wave ultrasound. *AIP Conf Proc* 2018; 1949: 090003.
17. Gavrić L. Computation of propagative waves in free rail using a finite element technique. *J Sound Vib* 1995; 185: 531–543.
18. Setschedi II, Loveday PW, Long CS, et al. Estimation of rail properties using semi-analytical finite element models and guided wave ultrasound measurements. *Ultrasonics* 2019; 96: 240–252.
19. Loveday PW, Long CS and Ramatlo DA. Mode repulsion of ultrasonic guided waves in rails. *Ultrasonics* 2018; 84: 341–349.
20. Loveday PW. Analysis of piezoelectric ultrasonic transducers attached to waveguides using waveguide finite elements. *IEEE T Ultrason Ferr* 2007; 54: 2045–2051.
21. Loveday PW. Simulation of piezoelectric excitation of guided waves using waveguide finite elements. *IEEE T Ultrason Ferr* 2008; 55: 2038–2045.
22. Ramatlo DA, Wilke DN and Loveday PW. Development of an optimal piezoelectric transducer to excite guided waves in a rail web. *NDT&E Int* 2018; 95: 72–81.
23. Jeong DY. *Correlations between rail defect growth data and engineering analyses, Part II: field tests*. Cambridge, MA: Volpe National Transportation Systems Center, 2003.
24. Jeong DY. *Correlations between rail defect growth data and engineering analyses, Part II: laboratory tests*. Cambridge, MA: Volpe National Transportation Systems Center, 2003.
25. Benmeddour F, Treyssède F and Laguerre L. Numerical modeling of guided wave interaction with non-axisymmetric cracks in elastic cylinders. *Int J Solids Struct* 2011; 48: 764–774.
26. Long CS and Loveday PW. Prediction of guided wave scattering by defects in rails using numerical modelling. *AIP Conf Proc* 2014; 1581: 240–247.
27. Holmes C, Drinkwater BW and Wilcox PD. Post-processing of the full matrix of ultrasonic transmit-receive array data for non-destructive evaluation. *NDT&E Int* 2005; 38: 701–711.
28. Wilcox PD. Guided-wave array methods. In: Boller C, Chang FK and Fujino Y (eds) *Encyclopedia of structural health monitoring*. Chichester: John Wiley & Sons, 2008, p. 1305.
29. Wilcox PD. A rapid signal processing technique to remove the effect of dispersion from guided wave signals. *IEEE T Ultrason Ferr* 2003; 50: 419–427.
30. Croxford AJ, Wilcox PD, Drinkwater BW, et al. Strategies for guided-wave structural health monitoring. *Proc R Soc Lond A Math* 2007; 463: 2961–2981.
31. Moustakidis S, Kappatos V, Karlsson P, et al. An intelligent methodology for railways monitoring using ultrasonic guided waves. *J Nondestruct Eval* 2014; 33: 694–710.
32. Hyvarinen A and Oja E. Independent component analysis: algorithms and applications. *Neural Network* 2000; 13: 411–430.